The conserved ER-transmembrane protein TMEM39A coordinates with vesicular COPII to promote collagen secretion and prevent ER stress

Running title: The TMEM39A protein family is essential for collagen secretion

Zhe Zhang[1], Shuo Luo[1], Guilherme Oliveira Barbosa[1], Meirong Bai[1], Thomas B. Kornberg[1,2] and Dengke K. Ma[1, 3, *]

[1]Cardiovascular Research Institute, University of California San Francisco, San Francisco, CA 94158

[2]Department of Biochemistry and Biophysics, University of California San Francisco, San Francisco, CA 94158

[3]Department of Physiology, University of California San Francisco, San Francisco, CA 94158

*Correspondence: Dengke.Ma@ucsf.edu

Abstract

Dysregulation of collagen production and secretion contributes to aging and tissue fibrosis of major organs. How premature collagen proteins in the endoplasmic reticulum (ER) route in specialized vesicles for secretion remains to be fully elucidated. Here, we report that TMEM39, an ER-localized transmembrane protein, regulates production and secretory cargo trafficking of procollagen. We identify the *C. elegans* orthologue TMEM-39 from an unbiased RNAi screen and show that deficiency of *tmem-39* leads to striking defects in cuticle collagen production and constitutively high ER stress response. RNAi knockdown of the *tmem-39* orthologue in *Drosophila* causes similar defects in collagen secretion in fat body cells. The cytosolic domain of the human orthologue TMEM39A binds to Sec23A, a vesicle coat protein that drives collagen secretion and vesicular trafficking. We propose that roles of TMEM39 in collagen secretion and preventing ER stress are likely evolutionarily conserved.

Keywords

TMEM-39, Sec23A, Collagen, Fibrosis, COPII vesicles

Introduction

Collagen is the major molecular component of connective tissues, and the most abundant protein in animals (Shoulders and Raines, 2009). Collagen dysregulation causes many human disorders, including autoimmune diseases, brittle bone diseases (too little collagen), tissue fibrosis (too much collagen) and ageing (Ewald et al., 2015; Humphreys, 2018; McKleroy et al., 2013; Murtha et al., 2017; Timpane et al., 2016; Wynn and Ramalingam, 2012). The multi-step biosynthesis of mature collagen by the cell is a complex process and involves procollagen gene transcription and protein translation, posttranslational modification, assembly into trimers inside the endoplasmic reticulum (ER), vesicular secretion from ER, extracellular peptide cleavage and cross-linking into collagen fibers (Mienaltowski and Birk, 2014; Shoulders and Raines, 2009).

Specific mechanisms responsible for secretion of procollagen still remain poorly understood. In general, specialized intracellular vesicles defined by the coat protein complex II (COPII) transport most secreted proteins, including procollagen, from the ER to the Golgi apparatus (Barlowe and Helenius, 2016; Jensen and Schekman, 2011). Sec23, Sec24, Sec13 and Sec31 comprise key COPII coat proteins, while the transport protein particle (TRAPP) complex acts a key tethering factor for COPII vesicle in route to the Golgi (Barlowe, 2020; Barrowman et al., 2010; D'Arcangelo et al., 2013). Typical COPII vesicles are 60 to 80 nm in diameter, which is not sufficient for transporting procollagen trimers with up to 300 to 400 nm in length (Malhotra and Erlmann, 2015). In mammals, large-size COPII-coated vesicles may transport procollagen from the ER

to the Golgi apparatus. TANGO1, a transmembrane protein at the ER exit site, is a key linker to mediate formation of specialized collagen-transporting vesicle and recruitment of procollagen (Malhotra and Erlmann, 2015; Malhotra et al., 2015; Santos et al., 2015). The N-terminal SH3-like domain of TANGO1 binds to the collagen chaperone HSP47 in the ER lumen, recruiting procollagens to the ER exit site (Ito and Nagata, 2019). Its C-terminal proline-rich domain (PRD) servers as a COPII receptor by interacting with the inner shell of Sec23/Sec24 (Wilson et al., 2011). The coil-coil domain of TANGO1 forms a stable complex with cTAE5 and SEC12, which is particularly enriched around large COPII carriers for procollagen (Yuan et al., 2018). Through its membrane helices, TANGO1 organizes ER exit sites by creating a lipid diffusion barrier and an export conduit for collagen (Raote et al., 2020). While requirement of TANGO1 for secretion may depend on specific collagen types, it remains unclear whether TANGO1's functions are broadly conserved in all animals (Matsui et al., 2020; Zhang et al., 2020).

Caenorhabditis elegans produces over 180 collagen members that constitute the cuticle and basement membranes, encodes conserved homologs of COPII/TRAPP proteins, yet lacks apparent TANGO1 homologs (Chioran et al., 2017; Kramer, 2005; Page and Johnstone, 2007; Teuscher et al., 2019). This indicates that evolutionarily conserved and TANGO1-independent mechanisms may exist in *C. elegans* to regulate procollagen secretion. From a genome-wide RNAi screen for genes affecting ER stress response, we previously identified *tmem-131* that defines a broadly conserved family of proteins important for procollagen assembly and secretion (Zhang et al., 2020). Mutations in specific collagen genes, conserved COPII/TRAPP-encoding homologues,

and impairment of collagen biosynthetic pathway components are known to result in a range of phenotypes including ER stress response, abnormal cuticle-associated morphology (Blister and Dumpy), and early death or growth arrest (Page and Johnstone, 2007). *tmem-131* mutants exhibit such phenotypes typical for genes required for collagen secretion (Zhang et al., 2020), while many other genes of unknown functions from our initial screen remain uncharacterized.

Here, we characterize another *C. elegans* gene *tmem-39* that encodes an ER transmembrane protein and is essential for cuticle collagen production. The deficiency of TMEM-39 protein in *C. elegans* impairs cuticle integrity and secretion of COL-19, an adult-specific cuticle collagen protein (Thein et al., 2003). We show that the *Drosophila* ortholog of *tmem-39, CG13016,* is also essential for collagen secretion. From yeast-two-hybrid (Y2H) screen, we find that the cytoplasmic loop domain of human TMEM39A binds to Sec23A, the inner shell component of the COPII coating complex. We demonstrate that SEC-23 and other COPII proteins are also essential for collagen secretion in *C. elegans*. Our findings suggest that TMEM39 coordinates with TMEM131 and COPII transport vesicles in the ER, and its roles in collagen secretion and preventing ER stress are likely evolutionarily conserved in multicellular animals.

Results

Genome-wide RNAi screen identifies *tmem-39* regulating ER stress response in *C. elegans*

We identified *D1007.5*, the sole *tmem-39* homologue in *C. elegans*, from a genome-wide RNAi screen for genes affecting the abundance of transgenic reporter *asp-*

*17*p::GFP, which is up-regulated by temperature stress and down-regulated by ER stress (Zhang et al., 2020). RNAi against *tmem-39* fully suppressed the *asp-17*p::GFP reporter expression (Fig. 1A). Ensembl gene tree analysis shows that TMEM39 family proteins are evolutionarily conserved from *C. elegans* to humans (Fig. 1B). Multiple human genetic studies have identified the human homologue *TMEM39A* as a susceptibility locus for various autoimmune diseases (Tran et al., 2017). TMEM39A is also overexpressed in glioblastoma cells and considered as a brain tumor-specific marker (Park et al., 2017). A recent study reported that TMEM39A is an ER-localized transmembrane protein that regulates autophagy (Miao et al., 2020). How TMEM-39 regulates ER stress response remains unknown.

In this work, we first confirmed that RNAi against *tmem-39* in *C. elegans* caused a fully penetrant and strong up-regulation of *hsp-4*p::GFP in hypodermis (Fig. 1C). *hsp-4*p::GFP is a well-established reporter for unfolded protein response (UPR) caused by ER stress in *C. elegans* (Harding et al., 2003). Loss-of-function of IRE-1, an ER stress-sensing protein, abolished *hsp-4*p::GFP induction in *tmem-39* RNAi treated animals (Fig. 1D). To verify the *tmem-39* RNAi phenotype, we used CRISPR/Cas9 to generate a *C. elegans* null allele *dma258* carrying a 2750 bp deletion of the entire coding sequences (Fig. 1E, Table S1). *dma258* mutants exhibited abnormally elevated transcriptional level of *hsp-4*p::GFP (Fig. 1F). Besides constitutively activated *hsp-4*p::GFP transcription, we also noticed that TMEM-39 deficient animals by RNAi or *dma258* were small and dumpy. Together, these results suggest that TMEM-39 as an ER-localized transmembrane protein is required for maintaining normal homeostasis

of ER-resident proteins.

Loss of *tmem-39* impairs cuticle collagen secretion in *C. elegans*

To identify potential protein clients in the ER regulated by TMEM-39, we examined 24 various translational reporters of ER-resident secreted and transmembrane proteins (Fig. S1, Table S2) and found that *tmem-39* RNAi knock-down strongly reduced COL-19::GFP reporter abundance (Fig. 2A). COL-19 is a *C. elegans* exoskeleton collagen that is secreted by the underlying hypoderm and required for integral structure of the cuticle (Page and Johnstone, 2007). The C-terminal GFP-tagged COL-19 reporter enables highly robust and tractable visualization of the cuticle morphology and to identify defects in the collagen production machinery (Thein et al., 2003).

Using confocal microscopy to characterize the structure of hypodermal cuticle, we found that in the control RNAi animals, COL-19::GFP is enriched in the hypoderm, constituting regular annular furrows and lateral alae of the cuticle (Fig. 2B). In the *tmem-39* RNAi animals, COL-19::GFP is apparently aggregated in the intracellular region of hypoderm, and largely absent in the cuticle (Fig. 2C). We further analyzed the abundance and composition of COL-19::GFP proteins by Western blot. Besides deficiency in overall COL-19::GFP abundance, *tmem-39* RNAi markedly increased the soluble “premature” monomeric procollagens, while decreased the insoluble fractions of cross-linked multimer and “mature” monomer of COL-19::GFP (Fig. 2D).

To examine possible involvement of *tmem-39* in collagen gene transcription, we used RNAi to knock-down *tmem-39* in animals with the *col-19*p::GFP transcriptional reporter

in which *GFP* expression is driven by the promoter of *col-19*. In contrast to the fully penetrant decrease of overall COL-19::GFP protein abundance, the transcriptional activity of the *col-19* promoter was not affected by *tmem-39* (Fig. 2C and 2E). We also evaluated the mRNA level of *col-19* by quantitative reverse transcription polymerase chain reaction (qRT-PCR) and found that the *dma258* mutant displayed a mild increase of *col-19* mRNA level, likely caused by a regulatory feedback loop in transcriptional regulation of collagen genes (Fig. 2F). The *dma258* mutant fully recapitulated the *tmem-39* RNAi phenotype in defective COL-19::GFP secretion (Fig. 2G).

There are two main collagen-enriched tissues in *C. elegans*, the cuticle (exoskeleton) and basement membranes (Kramer, 2005). *tmem-39* RNAi had no effect on the production of mCherry-tagged EMB-9 (Ihara et al., 2011), a Collagen IV α1 on basement membranes (Fig. S1T and Table S2). We found that loss of *tmem-39* specifically affected collagens in cuticle, as exemplified by COL-19:GFP, LON-3::GFP and COL-101::GFP (Fig. S2). Electron microscopy (EM) analysis revealed striking reduction of cuticle thickness in *dma258* mutants than in wild type (Fig. 2H). We also noticed that TMEM-39 deficient animals were small in size and dumpy, more sensitive to cuticle-disrupting osmotic stresses and developed more slowly. Taken together, these results demonstrate essential roles of TMEM-39 in collagen secretion, proper cuticle formation and preventing ER stress that is induced by premature collagen accumulation in *C. elegans*.

Evolutionarily conserved roles of TMEM39 family proteins for collagen secretion

TMEM39 family proteins are evolutionarily conserved among multicellular animals, and

invertebrate model organisms have one ortholog each, named *D1007.5* and *CG13016,* in *C. elegans* and *Drosophila*, respectively (Fig. 1B). We determined whether functions of TMEM39 family proteins in collagen secretion are evolutionarily conserved in *Drosophila.* We visualized collagen secretion in fat body cells of the *Lsp2> Col4a1:RFP* transgenic fly (Liu et al., 2017; Pastor-Pareja and Xu, 2011), and generated transgenic RNAi to knock-down *Drosophila CG13016*, the sole *TMEM39* ortholog (Fig. 3A). The physiological function of *Drosophila* fat body cells is to secrete collagen to the insect blood, hemolymph. Confocal microscopy analysis of COL4A1::RFP revealed that the Collagen type IV alpha 1::RFP proteins were strikingly accumulated in fat body cells of *CG13016* knock-down flies but not in control (Fig. 3B). Collagen accumulation caused by *CG13016* RNAi indicates the role of TMEM39 family proteins in collagen secretion is evolutionarily conserved also in *Drosophila*.

Since the sequence and function of TMEM39 appear to be highly conserved, we next characterized the localization and protein interactors of human TMEM39A. The vertebrate TMEM39 family consists of two paralogues, TMEM39A and TMEM39B (Park et al., 2017). The *TMEM39B* gene is only conserved in vertebrates, and is likely produced by the duplication of an ancestral form of *TMEM39A* (Kumar et al., 2017). Consistent with a recent study (Miao et al., 2020), our confocal imaging of Hela cells transiently transfected with reporters of GFP::TMEM39A and mCherry-tagged ER markers indicated that TMEM39A localized to the ER (Fig. 4A). Interestingly, TMEM39B appears to interact with the SARS-CoV-2 ORF9C protein (Gordon et al., 2020), which localizes to ER-derived vesicles in HeLa cells (Baruah et al., 2020).

Human TMEM39A cytoplasmic loop domain interacts with Sec23A

Predicted by the TOPCONS program, TMEM-39 contains putatively eight transmembrane segments and two large cytoplasmic loops (Fig. 4B). We further used the Y2H screen to search for human proteins that could interact with the conserved first loop domain (198-298 a.a.) and the second loop domain (337-420 a.a.) of TMEM39A (Fig. 4C). Among the prey cDNA clones identified from the Y2H, Sec23A was confirmed to interact with the second loop domain of TMEM39A (Fig. 4D).

The cDNA clone from the Y2H library encodes the C-terminal 583-765 a.a. of Sec23A, encompassing the Gelsolin repeat and C-terminal actin depolymerization factor-homology domain (Fig. 4C). Sec23A is a core component of the COPII vesicle coating complex, which forms SEC23-SEC24 heterodimers in the inner shell of the COPII coat to select specific cargo molecules (Bi et al., 2002; Khoriaty et al., 2018). Mutations in human Sec23A cause an autosomal recessive disease, named Cranio-lenticulo-sutural dysplasia (CLSD) (Khoriaty et al., 2018). The disease manifests with skeletal abnormalities, dysmorphic facial features and calvarial hypomineralization, features thought to result from defects in collagen secretion (Boyadjiev et al., 2011). Consistent with recent studies using the CoIP assay to demonstrate association between TMEM39A and Sec23A (Miao et al., 2020), we found that TMEM39A interacted with Sec23A but not Sec24D in Y2H assays (Fig. 4D). These results indicate that the TMEM39A cytoplasmic loop domain interacts with Sec23A, which forms an inner-shell heterodimer with Sec24 to select procollagen proteins destined for secretion.

We next examined the loss-of-function phenotype of *sec-23*. RNAi knock-down of *sec-*

23, the *C. elegans* homolog of *Sec23A*, strongly reduced COL-19::GFP secretion in the cuticle and increased its aggregation in the intracellular region of hypoderm (Fig. 4E). RNAi of *sec-23* also led to strong *hsp-4*p::GFP induction indicating constitutively activated ER stress response (Fig. 4F). RNAi against genes encoding other components of COPII also recapitulated the COL-19::GFP defects and *hsp-4*p::GFP induction phenotype (Fig. 4E, 4F, S3-4 and Table 1). These results show that the loop region of TMEM39A specifically binds to the COPII inner-shell component Sec23A and its *C. elegans* homolog *sec-23* is also essential for collagen production *in vivo*.

Importance of the conserved YR motif in the TMEM39A cytoplasmic loop domain

By amino acid sequence alignment, we identified two Tyrosine-Arginine (YR) residues in the second cytoplasmic loop domain of TMEM39A that are highly evolutionarily conserved among all examined species from invertebrates to vertebrates (Fig. 5A). We hypothesize that the conserved YR motif is important for interaction between TMEM39A and Sec23A. To confirm the prediction, we substituted the YR motif of TMEM39A into Alanine-Alanine (AA). Using Y2H assays, we found that such substitution in TMEM39A strongly attenuated its interaction with Sec23A (Fig. 5B).

To determine whether the YR motif of TMEM-39 is physiologically important *in vivo*, we generated a *C. elegans* knock-in allele *dma312* carrying a precise replacement of YR residues into AA (Fig. 5C). Ce-YR replacement mutants recapitulated the *tmem-39(dma258)* or *tmem-39* RNAi phenotype and exhibited abnormally strong *hsp-4*p::GFP induction but did not affect the mRNA abundance of *col-19* (Fig. 5D). As mutations, including synonymous mutations, can alter the secondary structure of an

mRNA and affect its stability (Duan et al., 2003), we measured the overall mRNA abundance of *tmem-39* by qRT-PCR. We found that the YR-AA mutant slightly increased *tmem-39* mRNA levels, similarly as the null allele likely caused by a transcriptional feedback regulation (Fig. 5D). Together, our findings support the essential role of the YR motif in the cytoplasmic loop domain of TMEM39A for its interaction with Sec23, and homologues of both proteins are required for collagen secretion and preventing ER stress in *C. elegans* (Fig. 5E).

Discussion

Our study identifies an ER transmembrane protein TMEM-39 in *C. elegans* with essential roles in collagen secretion. Such roles are likely evolutionarily conserved in animals. We propose that the TMEM39 cytoplasmic loop domain binds to Sec23A as the core component of COPII coating complex to facilitate procollagen transport from ER to Golgi (Fig. 5E). Phenotypic similarities of losses of TMEM-39 and TMEM-131, another ER transmembrane protein we recently identified (Zhang et al., 2020), suggest that both proteins cooperate in collagen secretion by assembling premature collagen and recruiting COPII/TRAPPIII complexes for sequential ER-to-Golgi cargo transport.

By yeast-two-hybrid assays, we found that the TMEM39A cytoplasmic loop domain can interact with the Sec23A. RNAi knock-down of *sec-23* and most other COPII genes recapitulated the *tmem-39* loss-of-function phenotypes in constitutively high ER stress response, defective collagen secretion and sensitivity to osmolality stress in *C. elegans* (Table 1). However, we also noticed that RNAi knock-down of many COPII related

237 genes, such as *sec-23, sec-24.1, npp-20, sar-1, sec-12, rab-5 and trpp-8* caused more
238 severe phenotypes than *tmem-39* RNAi, leading to lethality or developmental arrest
239 that prevent collagen phenotype analysis (Table 1). However, treatment with these
240 RNAi starting from L4-stage for animals transferred from normal conditions to RNAi led
241 to robust COL-19::GFP phenotype (Fig. 4E and Fig. S3). Shorter duration of RNAi
242 treatment may explain milder collagen defective phenotype for *sec-31*, *npp-20* and
243 *sec-12* (Fig. S3E, H and I). Compared with most COPII-related genes, *tmem-39* null
244 mutants exhibit similar collagen secretion defects but are nonetheless viable,
245 supporting the notion that TMEM-39 acts with COPII in collagen secretion but may
246 have more specialized roles in facilitating secretion of specific client proteins including
247 collagen COL-19 and the PtdIns(4)P Phosphatase SAC1 (Miao et al., 2020).

248 Besides Sec23A, additional interactors, such as Dctn6, was also identified from Y2H
249 screens with the TMEM39A cytoplasmic domain as bait. We verified the interaction
250 between full-length Dctn6 (1-190 a.a.) and TMEM39A (337-420 a.a.) (Fig. 4D). DCTN6
251 was identified as a subunit of the dynactin protein complex (Eckley et al., 1999).
252 Interestingly, dynactin is an essential cofactor of cytoplasmic dynein motor to transport
253 a variety of cargos and organelles along the microtubule-based cytoskeleton (Reck-
254 Peterson et al., 2018; Urnavicius et al., 2015). In mammalian cells, ER-to-Golgi
255 transport proceeds by cargo assembly into COPII-coated ER export sites (ERES)
256 followed by vesicular/tubular transport along microtubule tracks toward the Golgi in a
257 dynein/dynactin-dependent manner (Watson et al., 2005). Sec23p directly interacts
258 with the dynactin complex (Watson et al., 2005), indicating that TMEM39A may also

participate in a Sec23/DCTN6 complex to facilitate COPII coat assembly and subsequent dynein/dynactin-dependent transport. Test of this model and determination of the underlying mechanism in relation to TMEM131's role in collagen secretion await further investigations.

Mammalian genomes encode two TMEM39 family proteins,TMEM39A and TMEM39B. *TMEM39A* is a susceptibility locus associated with various autoimmune diseases and highly up-regulated in brain tumors (Park et al., 2017; Tran et al., 2017). TMEM39B was recently found to interact with the SARS-CoV-2 ORF9C protein, which localizes to ER-derived vesicles (Baruah et al., 2020; Gordon et al., 2020). It remains unclear whether *TMEM39A* and *TMEM39B* exhibit functional redundancy in collagen secretion or pathological processes in human diseases. With single *tmem39* orthologue for each, model organisms *C. elegans* and *Drosophila* may continue to provide insights into functions and mechanisms of action of this protein family. Future elucidation of novel and evolutionarily conserved roles of mammalian TMEM39 proteins in physiological and pathological processes will likely lead to therapeutic targets and strategies for alleviating diseases associated with this protein family in humans.

275 **Materials and Methods**

276 **Worm Strains**

277 The Bristol N2 strain was used as the wild type strain, and genotypes of other strains
278 used are as follow: *zcIs4* [*hsp-4*p::GFP] V, *ire-1(zc14)* II; *zcIs4* V, *dmaIs10* [*asp-*
279 *17*p::GFP; *unc-54*p::mCherry] X and *kaIs12* [*col-19*::GFP], *tmem-39(dma258)* and
280 *tmem-39(dma312)* I. Extrachromosomal array transgenic strains *dmaEx169* [*rpl-*
281 *28*p::T19D2.1::mCherry; *unc-122*p::GFP], *dmaEx153* [*rpl-28*p::Y73E7A.8::mCherry;
282 *unc-122*p::GFP], and *dmaEx152* [*rpl-28*p::F23H12.5::mCherry; *unc-122*p::GFP] were
283 generated as extrachromosomal arrays as described (Mello et al., 1991).

284 The precise *tmem-39(dma258)* knock-out strain was generated by CRISPR/Cas9
285 methods (Zhao et al., 2014; Zhao et al., 2016), and *tmem-39(dma312)* YR→AA was
286 generated by the amplified sgRNA method (Ward, 2015). Translational fluorescent
287 reporters used by *tmem-39* RNAi knock-down to identify a phenotype include: *bcIs39*
288 [*lim-7*p::*ced-1*::GFP+*lin-15*(+)], *caIs618* [*eff-1*p::*eff-1*::GFP], *dnSi4* [*gna-1*p::GFP +
289 Cbr-*unc-119*(+)], *juEx1111* [*spon-1*::vGFP], *lrp-1(ku156)eqIs1* [*lrp-1*p::*lrp-1*::GFP] I; *rrf-*
290 *3(pk1426)* II, *muIs49* [*egl-20*::GFP+*unc-22*(+)], *nIs590* [*fat-7*p::*fat-7*::GFP], *nuIs26* [*cat-*
291 *1*::GFP], *osIs60* [*unc-5*4p::*mig-23*::GFP; *unc-119*(+)], *osIs66* [*myo-3*p::eGFP::*wrk-1*],
292 *sqIs11* [*lgg-1*p::mCherry::GFP::*lgg-1*+*rol-6*(+)], *osIs77* [*unc-54*p::RFP::SP12;*unc-*
293 *119*(+)], *pwIs503* [*vha-6*p::*mans*::GFP+Cbr-*unc-119*(+)], *qyIs44* [*emb-9*p::*emb-*
294 *9*::mCherry], *rhIs23* [GFP::*him-4*], *veIs13 [col-19::GFP + rol-6(+)] V; let-7(mn112) unc-*
295 *3(e151) X; mgEx725 [lin-4::let-7 + ttx-3::RFP],* *vkEx1243* [*nhx-2*p::ubiquitin-
296 V::mCherry+*myo-2*p::GFP], *vkEx1256* [*nhx-2*p::*cpl-1*::YFP], *vkEx1260* [*nhx-2*p::*cpl-*

297 *1*::YFP], *vkEx1879* [*nhx-2*p::*cpl-1*(W32A Y35A)::YFP] and *xnIs96* [*hmr-1*p::*hmr-*
298 *1*::GFP].

299 **Worm maintenance**

300 We used standard methods to grow *C. elegans* strains on *E. coli* at 20 °C, and animals
301 were maintained in standard nematode growth medium (NGM) plates (Brenner, 1974).
302 Worms were synchronized by bleaching the gravid adults, and RNAi feeding induced
303 knock-down was performed as previously described (Kamath and Ahringer, 2003). For
304 RNAi colonies that show lethality or larvae arrest phenotype, around 20-30 P0 L4
305 animals were transferred from normal NGM plates to RNAi plates, and grew for 2-3
306 days to observe the P0 phenotype.

307 **Imaging**

308 Digital automated epifluorescence microscopes (EVOS, Life Technologies) and SPE
309 confocal microscope (Leica) were used to obtain fluorescence images. Animals at the
310 same stage were randomly picked from the plate, and transferred to an 4% agar pad
311 with 10 mM sodium azide and 1 mM levamisole in M9 solution (31742-250MG, Sigma-
312 Aldrich) on a slide for imaging. Identical setting and conditions were used to compare
313 experimental groups with control.

314 **Western blot analysis of proteins**

315 Animals at the same stage from the control and experiment groups were picked (N>30)
316 into 20 μL Laemmli Sample Buffer and lysed directly for Western blot analysis. Protein
317 samples were run with 15% SDS-PAGE (Bio-Rad, 4561084), and then transferred to

318 the nitrocellulose membrane (Bio-Rad, 1620167). The membranes were detected by
319 antibodies against GFP (A02020, Abbkine), Tubulin (Sigma, T5168) and H3 (Abcam,
320 ab1791).

321 **Quantitative RT-PCR**

322 Worm total RNA was extracted by following the protocols of Quick-RNA MiniPrep kit
323 (Zymo Research, R1055). And cDNA was reverse transcribed by the reverse
324 transcriptase mix kit (BioTools, B24408). Using SYBR Green Supermix (Thermo Fisher
325 Scientific, FERK1081), the Real-time PCR was performed by on Roche LightCycler96
326 (Roche, 05815916001) system. Ct values of specific genes were normalized to the *C.*
327 *elegans* housekeeping gene *act-1* levels. Results are presented as fold changes to
328 respective references. Statistical significance was determined with t-test, using
329 GraphPad Prism 7. Primer sequences are listed in Supplementary Table 1B.

330 ***Drosophila* experiments**

331 Fly strains included: UAS-Cg25C:RFP.2.1/CyO; Lsp2-Gal4/TM6B, and UAS-
332 CG13016_dsRNA (Vienna Drosophila Resource Center ID# 42509/GD). Lsp2-Gal4
333 specifically expresses in the fat body. Flies expressing Collagen:RFP in fat body were
334 crossed to either wild type or UAS-CG13016_dsRNA flies. Wandering stage third instar
335 larvae were picked out. Fat body was dissected and fixed in PFA 4%, stained with
336 DAPI, and mounted for imaging by confocal microscopy.

337 **Yeast two hybrid assay**

338 The cDNA coding sequences of the first and second cytoplasmic loop domain of
339 human TMEM39A were cloned into the pGBKT7 vector and screened against a

340 normalized universal human cDNA library (Clontech, 630481), following instructions of
341 the Matchmaker® Gold Yeast Two-Hybrid System (Clontech, 630489). Verification of
342 positive colonies was achieved by co-transforming wild-type or YR-mutant TMEM39A
343 loop domain (in pGBKT7 Vector) with genes of interest (in pGADT7 Vector) following
344 the instruction of YeastMaker™ Yeast Transformation System 2 (Clontech, 630439) as
345 well as plasmids from re-cloned cDNA.

346 **Fluorescent imaging of Hela cells**

347 Hela cells were seeded in 24-well plates with cover glass, each with three replicates
348 (Fisher Scientific, 22293232). Cells were transiently transfected with GFP-tagged
349 human *TMEM39A* full-length cDNA in the FUGW plasmid backbone, and the
350 endoplasmic reticulum localization marker mCherry-ER-3 (Addgene: 55041) for 2 days.
351 After 1xPBS washing for once, cells were treated by 4% formaldehyde solution for 10
352 mins. With 1xPBS washing for three times, cells were treated with 0.2% Triton X-100
353 in 1xPBS solution for 15 mins. Following 1xPBS washing for three times, the cover
354 slide with cell samples was sealed on the microscope slide with Fluoroshield Mounting
355 Medium with DAPI (Thermo Fisher Scientific, NC0200574) for imaging by confocal
356 microscopy.

Acknowledgements

We thank the *Caenorhabditis* Genetics Center for *C. elegans* strains. The work was supported by NIH grants R01GM117461, Pew Scholar Award, and Packard Fellowship in Science and Engineering (D.K.M). We thank Drs. Hong Zhang, Kamran Atabai and Matthew Shoulders for discussion and Dr. Jose Pastor-Pareja for the transgenic *Drosophila* line: w*; UAS-Cg25C.RFP.2.1. The authors declare that they have no competing interests and all participated experimental design, execution or data interpretation and analysis. Z.Z. and D.K.M wrote the paper.

Abbreviations

a.a., amino acid; CLSD, Cranio-lenticulo-sutural dysplasia; COPII, Coat protein complex II; C-terminus, carboxylic acid-terminus; EM, Electron microscopy; ER, endoplasmic reticulum; ERES, ER export sites; GWASs, Genome-wide association studies; NGM, nematode growth media; nt, nucleotide; N-terminus, amino-terminus; PRD, proline-rich domain; qRT-PCR, quantitative reverse transcription polymerase chain reaction TRAPP, transport protein particle; Y2H, yeast-two-hybrid;

Compliance with ethics guidelines

Zhe Zhang, Shuo Luo, Guilherme Oliveira Barbosa, Meirong Bai, Thomas B. Kornberg and Dengke K. Ma declare that they have no conflict of interests.

All institutional and national guidelines for the care and use of laboratory animals were followed.

377 **References**

378 Barlowe, C. (2020). Twenty-five years after coat protein complex II. Mol Biol Cell *31*,
379 3-6.

380 Barlowe, C., and Helenius, A. (2016). Cargo Capture and Bulk Flow in the Early
381 Secretory Pathway. Annu Rev Cell Dev Biol *32*, 197-222.

382 Barrowman, J., Bhandari, D., Reinisch, K., and Ferro-Novick, S. (2010). TRAPP
383 complexes in membrane traffic: convergence through a common Rab. Nat Rev Mol
384 Cell Biol *11*, 759-763.

385 Baruah, C., Devi, P., and Sharma, D.K. (2020). Sequence analysis and structure
386 prediction of SARS-CoV-2 accessory proteins 9b and ORF14: evolutionary analysis
387 indicates close relatedness to bat coronavirus.

388 Bi, X., Corpina, R.A., and Goldberg, J. (2002). Structure of the Sec23/24-Sar1 pre-
389 budding complex of the COPII vesicle coat. Nature *419*, 271-277.

390 Boyadjiev, S.A., Kim, S.D., Hata, A., Haldeman-Englert, C., Zackai, E.H., Naydenov,
391 C., Hamamoto, S., Schekman, R.W., and Kim, J. (2011). Cranio-lenticulo-sutural
392 dysplasia associated with defects in collagen secretion. Clin Genet *80*, 169-176.

393 Brenner, S. (1974). The genetics of Caenorhabditis elegans. Genetics *77*, 71-94.

394 Chioran, A., Duncan, S., Catalano, A., Brown, T.J., and Ringuette, M.J. (2017).
395 Collagen IV trafficking: The inside-out and beyond story. Dev Biol *431*, 124-133.

396 D'Arcangelo, J.G., Stahmer, K.R., and Miller, E.A. (2013). Vesicle-mediated export
397 from the ER: COPII coat function and regulation. Biochim Biophys Acta *1833*, 2464-
398 2472.

399 Duan, J., Wainwright, M.S., Comeron, J.M., Saitou, N., Sanders, A.R., Gelernter, J.,
400 and Gejman, P.V. (2003). Synonymous mutations in the human dopamine receptor D2
401 (DRD2) affect mRNA stability and synthesis of the receptor. Hum Mol Genet *12*, 205-
402 216.

403 Eckley, D.M., Gill, S.R., Melkonian, K.A., Bingham, J.B., Goodson, H.V., Heuser, J.E.,
404 and Schroer, T.A. (1999). Analysis of dynactin subcomplexes reveals a novel actin-
405 related protein associated with the arp1 minifilament pointed end. J Cell Biol *147*, 307-
406 320.

407 Ewald, C.Y., Landis, J.N., Porter Abate, J., Murphy, C.T., and Blackwell, T.K. (2015).
408 Dauer-independent insulin/IGF-1-signalling implicates collagen remodelling in
409 longevity. Nature *519*, 97-101.

410

411 Gordon, D.E., Jang, G.M., Bouhaddou, M., Xu, J., Obernier, K., White, K.M., O'Meara,
412 M.J., Rezelj, V.V., Guo, J.Z., Swaney, D.L., *et al.* (2020). A SARS-CoV-2 protein
413 interaction map reveals targets for drug repurposing. Nature *583*, 459-468.

414 Harding, H.P., Zhang, Y., Zeng, H., Novoa, I., Lu, P.D., Calfon, M., Sadri, N., Yun, C.,
415 Popko, B., Paules, R., *et al.* (2003). An integrated stress response regulates amino
416 acid metabolism and resistance to oxidative stress. Mol Cell *11*, 619-633.

417 Humphreys, B.D. (2018). Mechanisms of Renal Fibrosis. Annu Rev Physiol *80*, 309-
418 326.

419 Ihara, S., Hagedorn, E.J., Morrissey, M.A., Chi, Q., Motegi, F., Kramer, J.M., and
420 Sherwood, D.R. (2011). Basement membrane sliding and targeted adhesion remodels
421 tissue boundaries during uterine-vulval attachment in Caenorhabditis elegans. Nat Cell
422 Biol *13*, 641-651.

423 Ito, S., and Nagata, K. (2019). Roles of the endoplasmic reticulum-resident, collagen-
424 specific molecular chaperone Hsp47 in vertebrate cells and human disease. J Biol
425 Chem *294*, 2133-2141.

426 Jensen, D., and Schekman, R. (2011). COPII-mediated vesicle formation at a glance.
427 Journal of cell science *124*, 1-4.

428 Kamath, R.S., and Ahringer, J. (2003). Genome-wide RNAi screening in
429 Caenorhabditis elegans. Methods *30*, 313-321.

430 Khoriaty, R., Hesketh, G.G., Bernard, A., Weyand, A.C., Mellacheruvu, D., Zhu, G.,
431 Hoenerhoff, M.J., McGee, B., Everett, L., Adams, E.J., *et al.* (2018). Functions of the
432 COPII gene paralogs SEC23A and SEC23B are interchangeable in vivo. Proc Natl
433 Acad Sci U S A *115*, E7748-E7757.

434 Kramer, J.M. (2005). Basement membranes. WormBook, 1-15.

435 Kumar, S., Stecher, G., Suleski, M., and Hedges, S.B. (2017). TimeTree: A Resource
436 for Timelines, Timetrees, and Divergence Times. Mol Biol Evol *34*, 1812-1819.

437 Liu, M., Feng, Z., Ke, H., Liu, Y., Sun, T., Dai, J., Cui, W., and Pastor-Pareja, J.C. (2017).
438 Tango1 spatially organizes ER exit sites to control ER export. J Cell Biol *216*, 1035-
439 1049.

440 Malhotra, V., and Erlmann, P. (2015). The pathway of collagen secretion. Annu Rev
441 Cell Dev Biol *31*, 109-124.

442 Malhotra, V., Erlmann, P., and Nogueira, C. (2015). Procollagen export from the
443 endoplasmic reticulum. Biochem Soc Trans *43*, 104-107.

444

445 Matsui, Y., Hirata, Y., Wada, I., and Hosokawa, N. (2020). Visualization of Procollagen
446 IV Reveals ER-to-Golgi Transport by ERGIC-independent Carriers. Cell Struct Funct
447 *45*, 107-119.

448 McKleroy, W., Lee, T.H., and Atabai, K. (2013). Always cleave up your mess: targeting
449 collagen degradation to treat tissue fibrosis. Am J Physiol Lung Cell Mol Physiol *304*,
450 L709-721.

451 Mello, C.C., Kramer, J.M., Stinchcomb, D., and Ambros, V. (1991). Efficient gene
452 transfer in C.elegans: extrachromosomal maintenance and integration of transforming
453 sequences. EMBO J *10*, 3959-3970.

454 Miao, G., Zhang, Y., Chen, D., and Zhang, H. (2020). The ER-Localized
455 Transmembrane Protein TMEM39A/SUSR2 Regulates Autophagy by Controlling the
456 Trafficking of the PtdIns(4)P Phosphatase SAC1. Mol Cell *77*, 618-632 e615.

457 Mienaltowski, M.J., and Birk, D.E. (2014). Structure, physiology, and biochemistry of
458 collagens. Adv Exp Med Biol *802*, 5-29.

459 Murtha, L.A., Schuliga, M.J., Mabotuwana, N.S., Hardy, S.A., Waters, D.W., Burgess,
460 J.K., Knight, D.A., and Boyle, A.J. (2017). The Processes and Mechanisms of Cardiac
461 and Pulmonary Fibrosis. Front Physiol *8*, 777.

462 Page, A.P., and Johnstone, I.L. (2007). The cuticle. WormBook, 1-15.

463 Park, J., Lee, H., Tran, Q., Mun, K., Kim, D., Hong, Y., Kwon, S.H., Brazil, D., Park, J.,
464 and Kim, S.H. (2017). Recognition of Transmembrane Protein 39A as a Tumor-Specific
465 Marker in Brain Tumor. Toxicol Res *33*, 63-69.

466 Pastor-Pareja, J.C., and Xu, T. (2011). Shaping cells and organs in Drosophila by
467 opposing roles of fat body-secreted Collagen IV and perlecan. Dev Cell *21*, 245-256.

468 Raote, I., Ernst, A.M., Campelo, F., Rothman, J.E., Pincet, F., and Malhotra, V. (2020).
469 TANGO1 membrane helices create a lipid diffusion barrier at curved membranes. Elife
470 *9*.

471 Reck-Peterson, S.L., Redwine, W.B., Vale, R.D., and Carter, A.P. (2018). The
472 cytoplasmic dynein transport machinery and its many cargoes. Nat Rev Mol Cell Biol
473 *19*, 382-398.

474 Santos, A.J., Raote, I., Scarpa, M., Brouwers, N., and Malhotra, V. (2015). TANGO1
475 recruits ERGIC membranes to the endoplasmic reticulum for procollagen export. Elife
476 *4*.

477 Shoulders, M.D., and Raines, R.T. (2009). Collagen structure and stability. Annu Rev
478 Biochem *78*, 929-958.

479 Teuscher, A.C., Jongsma, E., Davis, M.N., Statzer, C., Gebauer, J.M., Naba, A., and
480 Ewald, C.Y. (2019). The in-silico characterization of the Caenorhabditis elegans
481 matrisome and proposal of a novel collagen classification. Matrix Biology Plus *1*,
482 100001.

483 Thein, M.C., McCormack, G., Winter, A.D., Johnstone, I.L., Shoemaker, C.B., and
484 Page, A.P. (2003). Caenorhabditis elegans exoskeleton collagen COL-19: an adult-
485 specific marker for collagen modification and assembly, and the analysis of organismal
486 morphology. Dev Dyn *226*, 523-539.

487 Timpane, S., Brandling-Bennett, H., and Kristjansson, A.K. (2016). Autoimmune
488 collagen vascular diseases: Kids are not just little people. Clin Dermatol *34*, 678-689.

489 Tran, Q., Park, J., Lee, H., Hong, Y., Hong, S., Park, S., Park, J., and Kim, S.H. (2017).
490 TMEM39A and Human Diseases: A Brief Review. Toxicol Res *33*, 205-209.

491 Urnavicius, L., Zhang, K., Diamant, A.G., Motz, C., Schlager, M.A., Yu, M., Patel, N.A.,
492 Robinson, C.V., and Carter, A.P. (2015). The structure of the dynactin complex and its
493 interaction with dynein. Science *347*, 1441-1446.

494 Ward, J.D. (2015). Rapid and precise engineering of the Caenorhabditis elegans
495 genome with lethal mutation co-conversion and inactivation of NHEJ repair. Genetics
496 *199*, 363-377.

497 Watson, P., Forster, R., Palmer, K.J., Pepperkok, R., and Stephens, D.J. (2005).
498 Coupling of ER exit to microtubules through direct interaction of COPII with dynactin.
499 Nature cell biology *7*, 48-55.

500 Wilson, D.G., Phamluong, K., Li, L., Sun, M., Cao, T.C., Liu, P.S., Modrusan, Z.,
501 Sandoval, W.N., Rangell, L., Carano, R.A.*, et al.* (2011). Global defects in collagen
502 secretion in a Mia3/TANGO1 knockout mouse. J Cell Biol *193*, 935-951.

503 Wynn, T.A., and Ramalingam, T.R. (2012). Mechanisms of fibrosis: therapeutic
504 translation for fibrotic disease. Nat Med *18*, 1028-1040.

505 Yuan, L., Kenny, S.J., Hemmati, J., Xu, K., and Schekman, R. (2018). TANGO1 and
506 SEC12 are copackaged with procollagen I to facilitate the generation of large COPII
507 carriers. Proc Natl Acad Sci U S A *115*, E12255-E12264.

508 Zhang, Z., Bai, M., Barbosa, G.O., Chen, A., Wei, Y., Luo, S., Wang, X., Wang, B.,
509 Tsukui, T., Li, H.*, et al.* (2020). Broadly conserved roles of TMEM131 family proteins in
510 intracellular collagen assembly and secretory cargo trafficking. Sci Adv *6*, eaay7667.

511 Zhao, P., Zhang, Z., Ke, H., Yue, Y., and Xue, D. (2014). Oligonucleotide-based
512 targeted gene editing in C. elegans via the CRISPR/Cas9 system. Cell Res *24*, 247-
513 250.

514 Zhao, P., Zhang, Z., Lv, X., Zhao, X., Suehiro, Y., Jiang, Y., Wang, X., Mitani, S., Gong,
515 H., and Xue, D. (2016). One-step homozygosity in precise gene editing by an improved
516 CRISPR/Cas9 system. Cell Res *26*, 633-636.

517

518

519 **Figure legends**

520 **Fig. 1. TMEM-39 regulates ER stress response in *C. elegans*.** (A), Exemplar
521 fluorescence images for *asp-17*p::GFP with control and *tmem-39* RNAi. Scale bars: 20
522 µm. (B), Ensembl gene tree analysis for TMEM39 protein family and amino acid
523 sequence alignment among metazoan species (adapted from https://m.ensembl.org/).
524 (C-D), Exemplar fluorescence and bright-field images for the UPR reporter *hsp-*
525 *4*p::GFP with control and *tmem-39* RNAi in wild type (C) and *ire-1*(D) mutants. Scale
526 bars: 20 µm. (E), Schematic of *tmem-39* gene structure with the *dma258* deletion
527 generated by CRISPR-Cas9. Bold and underlined are sgRNA target sequence from
528 the *tmem-3*9 regions. The location of the deleted *tmem-39* is marked with "^",
529 generating a precise 2750 bp deletion. (F) qRT-PCR measurements of *hsp-4*p::GFP
530 mRNA levels in wild-type and *dma258* mutants. ***P < 0.001 (n ≥ 3 biological
531 replicates).

532 **Fig. 2. TMEM-39 is essential for collagen secretion and cuticle formation in *C.***
533 ***elegans*.** (A), Exemplar epifluorescence image of *col-19*::GFP with control and *tmem-*
534 *39* RNAi. Three to four animals were shown to indicate representative reporter
535 expression with around 50 animals observed. (B-C) Exemplar confocal fluorescence
536 images of COL-19::GFP with indicated phenotypic penetrance of control RNAi (B) and
537 *tmem-39* RNAi (C) in wild-type animals. Scale bars: 20 μm. (D), Exemplar Western
538 blot analysis of COL-19::GFP proteins from total lysates of wild type animals with
539 control and *tmem-39* RNAi. IB, immunoblotting. The arrow indicates soluble premature
540 monomers; triangles indicate insoluble mature monomers and cross-linked COL-
541 19::GFP. (E), Exemplar fluorescence images of *col-19* transcriptional reporter (*col-19*
542 promoter-driven GFP) with indicated phenotypic penetrance of control RNAi and
543 *tmem-39* RNAi in wild-type animals, indicating no significant difference in GFP
544 expression. Scale bars: 20 μm. (F), qRT-PCR quantification of endogenous col-19
545 mRNA levels in wild-type and *dma258* mutants. ***$P < 0.001$ ($n \geq 3$ biological
546 replicates).
547

548 **Fig. 3. Evolutionarily conserved roles of TMEM39 family proteins for collagen**
549 **secretion in *Drosophila*.** (A), Schematic of generating fat body cell specific CG13016
550 knock-down strains in *Drosophila.* Lsp2-Gal4 specifically expresses in the fat body.
551 Wandering stage third instar larvae were picked out for imaging analysis. The
552 *Drosophila* images are created by BioRender.com. (B), Exemplar confocal images of
553 transgenic *Drosophila* fat body cells showing collagen COL4A1 secretion is normal
554 with control RNAi (left), and collagen accumulation with *tmem39/CG13016* RNAi. scale
555 bar, 100 μm.

556

557

558

559

560

561

562 **Fig. 4. Human TMEM39A cytoplasmic loop domain interacts with Sec23A and**
563 **COPII components regulate collagen secretion in *C. elegans***. (A), Exemplar
564 confocal fluorescence images of HeLa cells co-transfected with GFP-tagged
565 TMEM39A and mCherry-tagged ER marker (ER3). Scale bars, 5 μm. (B) Schematic of
566 human TMEM39A transmembrane domain predicted by the TOPCONS program, with
567 cytosolic localization in red (two long cytoplasmic loop domains labeled with rectangles,
568 loop1 in green and loop2 in blue) and ER localization in blue. (C), Schematic of Y2H
569 screens identifying the human Sec23A C-terminal domain as a binder of the second
570 cytoplasmic loop domain of TMEM39A. (D), Y2H assays of yeast colony growth after
571 prey and bait vectors retransformation to verify the interaction of human Sec23A C-
572 termini (a.a. 583-765), Sec24D full length (a.a. 1-1032) and Dctn6 full length (a.a. 1-
573 190) with TMEM39A loop1 (a.a. 198-298) and loop2 (a.a. 337-420). (E-F) Exemplar
574 confocal fluorescence images of COL-19::GFP (E) and *hsp-4*p::GFP with indicated
575 phenotypic penetrance of wild-type with control RNAi and COPII components *sec-23*
576 and *trpp-3* RNAi. Scale bars: 20 μm.
577

578 **Fig. 5. The conserved YR motif in cytoplasmic loop region is essential for the**
579 **function of TMEM39A protein.** (A), Multiple sequence alignment of TMEM39A from
580 major representative animal species (by COBALT program), with conserved YR
581 residues indicated in the second cytoplasmic loop domains. (B), Y2H assays of yeast
582 colony growth after prey and bait vectors retransformation to verify the interaction
583 between human Sec23A C-termini (a.a. 583-765) with human wild type and YR mutant
584 TMEM39A cytoplasmic loop domain (a.a. 337-420). (C), Schematic of precise
585 replacement for YR motif coding sequence in *tmem-39* gene generated by CRISPR-
586 Cas9. (D), qRT-PCR measurements of endogenous *col-19*, *tmem-39* and *hsp-4*p::GFP
587 mRNA levels in wild-type and *tmem-39* YR mutants. ***$P < 0.001$ ($n \geq 3$ biological
588 replicates). (E), Schematic model showing TMEM39A regulation of collagen secretion.
589 The second cytoplasmic loop domain of TMEM39A interacts with the core COPII
590 coating component Sec23A. TMEM131 binds to COL1A2 to facilitate assembly of
591 procollagen trimers and TRAPP III activation of Rab GTPase, in coordination with
592 TMEM39A to promote the ER-to-Golgi transport of procollagen cargo in COPII. Uso1
593 interacts with the COPII vesicle to promote targeting to the Golgi apparatus.

594

595

Table 1. RNAi phenotypic analysis of COPII related genes in *hsp-4*p::GFP (ER stress) and COL-19::GFP (collagen) .

Gene	Description	ER	collagen	Phenotype
tmem-39	Recruit Sec23A	+++	----	Smaller, disrupting
tmem-131	Recruit TRAPPC8, procollagen	+++	----	Smaller, disrupting
sec-23	COPII component	+++	----	L1-L2 arrest
sec-24.1	COPII component	+++	----	L1-L2 arrest
sec-24.2	COPII component	N.D.	N.D.	N.D.
npp-20	Sec13, COP II component	+++	N.D.	L4 arrest, disrupting
sec-31	COPII component	+	N.D.	N.D.
sar-1	GTPase, interact with sec-12	+++	--	L4 arrest, disrupting
sec-12	GTP-binding Sar1 protein	+++	N.D.	L1-L2 arrest
rab-1	Rab GTPase	+++	----	L1-L2 arrest
trpp-3	TRAPPIII component	++	----	N.D.
trpp-6	TRAPPIII component	N.D.	----	N.D.
trpp-8	TRAPPIII component	N.D.	----	sterile
uso-1	USO1 vesicle transport factor	+++	N.D.	N.D.

+ indicates *hsp-4*p::GFP fluorescent reporter level induction, and – indicates COL-19::GFP level reduction under different RNAi conditions; qualitative changes were followed up by quantitative fluorescence (n≥ 50 biological replicates) and western blot analysis for verification. N.D., no difference.

604 **Fig. 1**

605

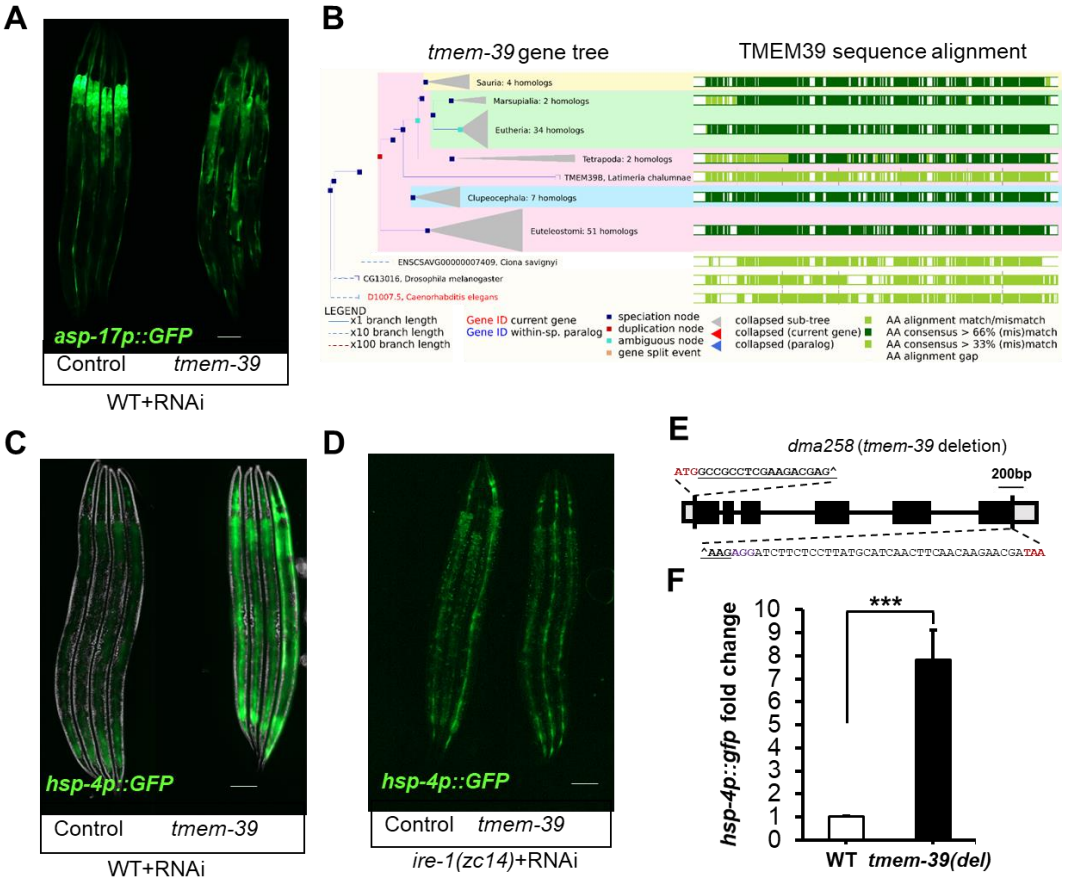

606

607

608

609 **Fig. 2**

610

611

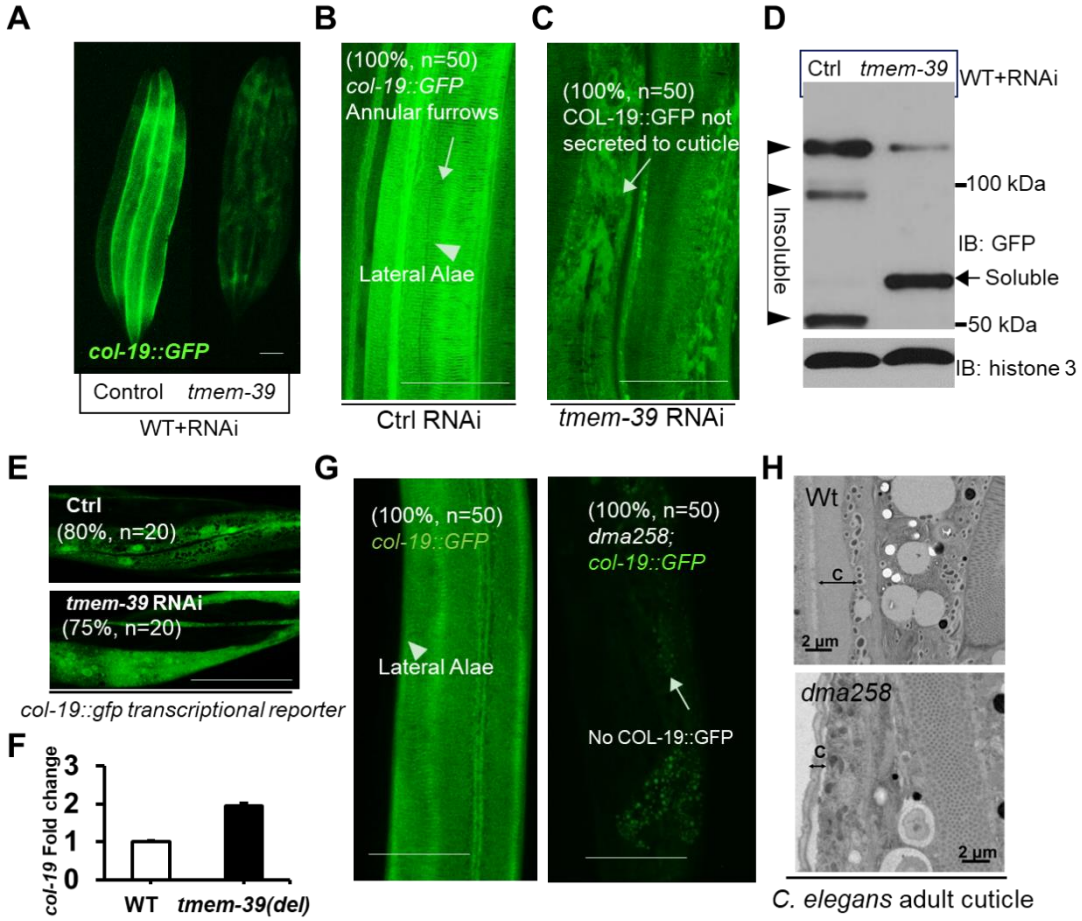

612

613

614

615 **Fig. 3**

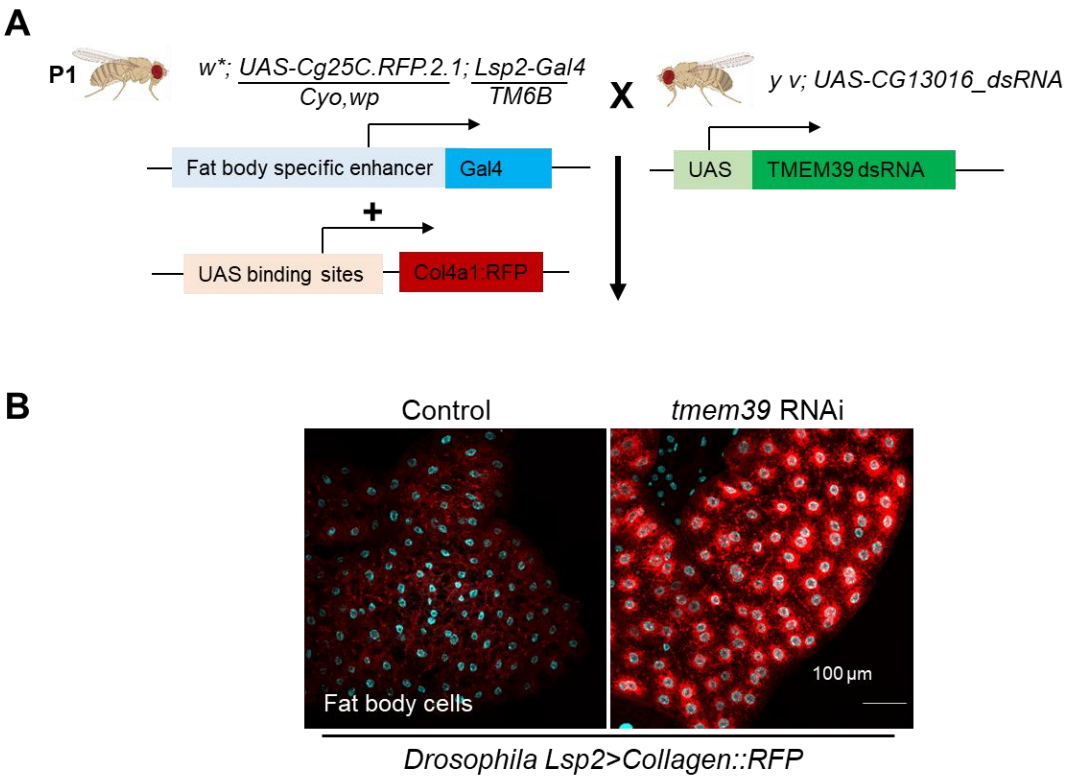
A
P1
w*; UAS-Cg25C.RFP.2.1; Lsp2-Gal4
Cyo,wp
TM6B
X
y v; UAS-CG13016_dsRNA
Fat body specific enhancer
Gal4
UAS
TMEM39 dsRNA
+
UAS binding sites
Col4a1:RFP
B
Control
tmem39 RNAi
Fat body cells
100 µm
Drosophila Lsp2>Collagen::RFP

616 **Fig. 4**

617

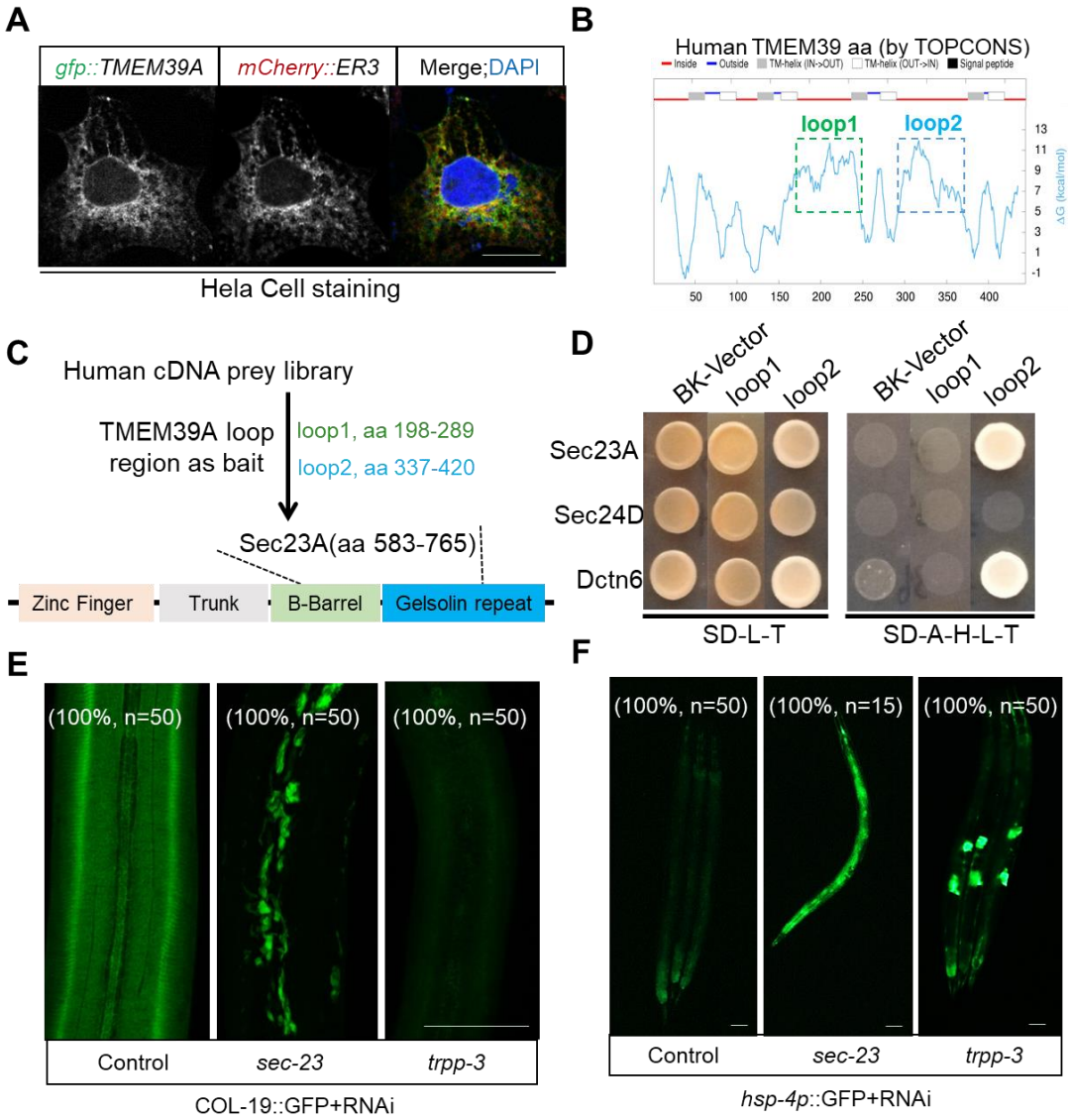
A
gfp::TMEM39A
mCherry::ER3
Merge;DAPI
Hela Cell staining
B
Human TMEM39 aa (by TOPCONS)
Inside
Outside
TM-helix (IN->OUT)
TM-helix (OUT->IN)
Signal peptide
loop1
loop2
ΔG (kcal/mol)
C
Human cDNA prey library
TMEM39A loop region as bait
loop1, aa 198-289
loop2, aa 337-420
Sec23A(aa 583-765)
Zinc Finger
Trunk
B-Barrel
Gelsolin repeat
D
BK-Vector
loop1
loop2
Sec23A
Sec24D
Dctn6
SD-L-T
SD-A-H-L-T
E
(100%, n=50)
(100%, n=50)
(100%, n=50)
Control
sec-23
trpp-3
COL-19::GFP+RNAi
F
(100%, n=50)
(100%, n=15)
(100%, n=50)
Control
sec-23
trpp-3
hsp-4p::GFP+RNAi

618 **Fig. 5**

619

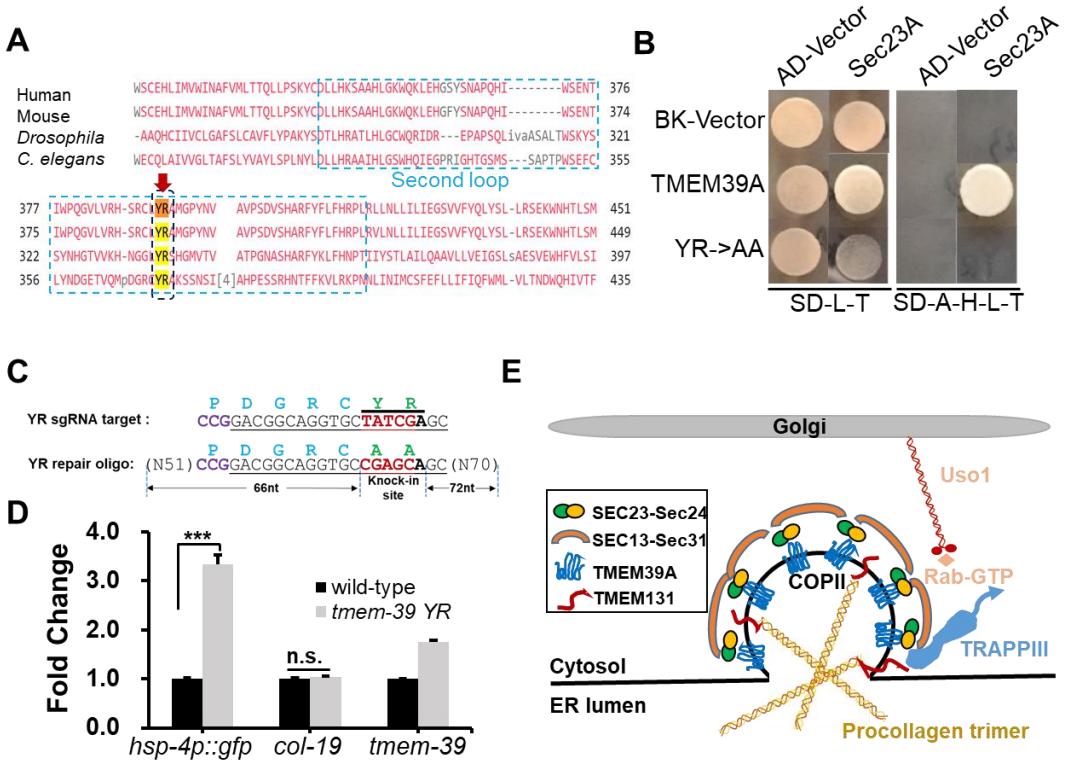

620

621

622 **Supplementary Materials**

623 **Figures. S1 to S4**

624 **Fig. S1**

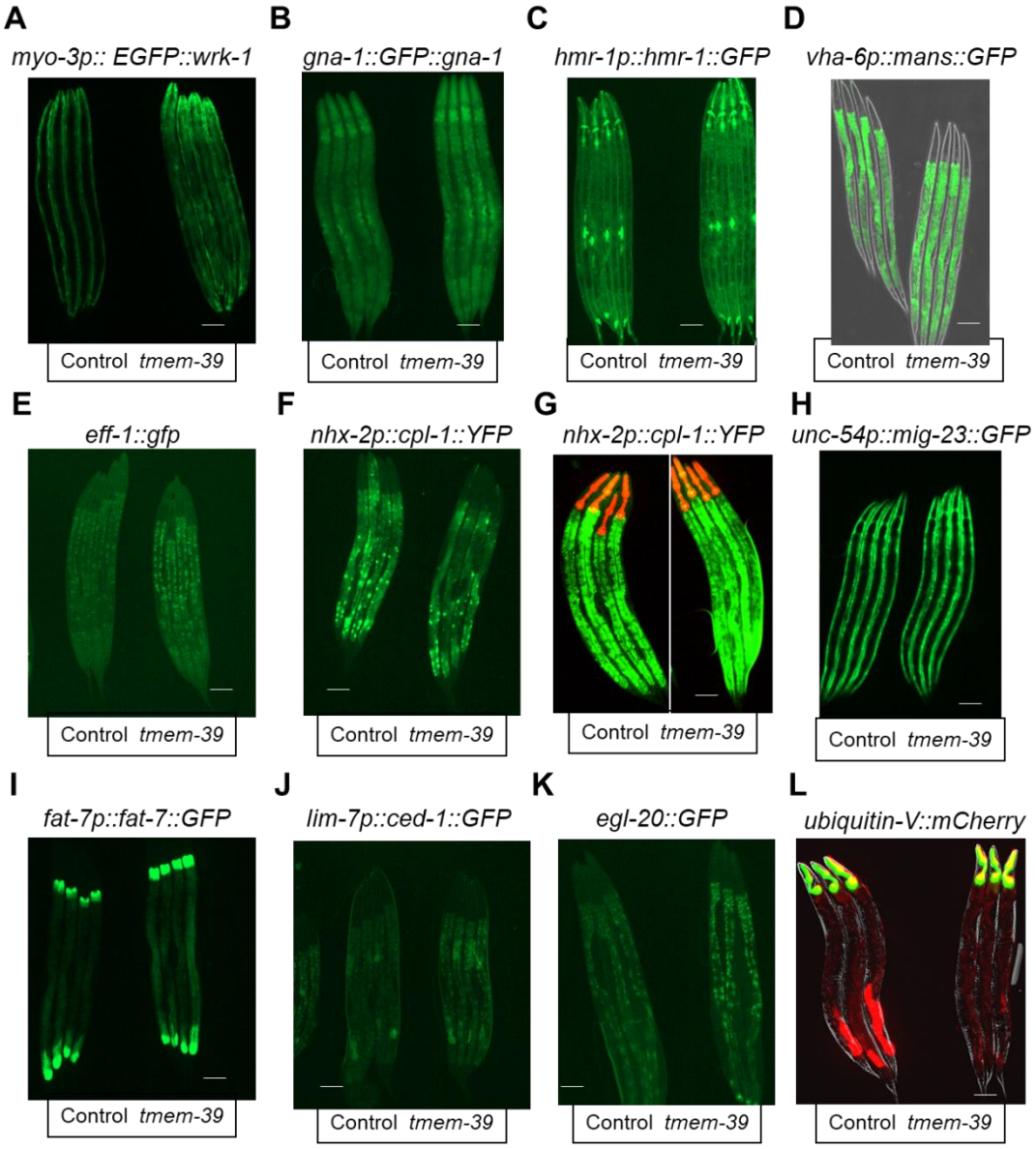

625

626

627

Refer to Extended Data Fig. S1 (continued)

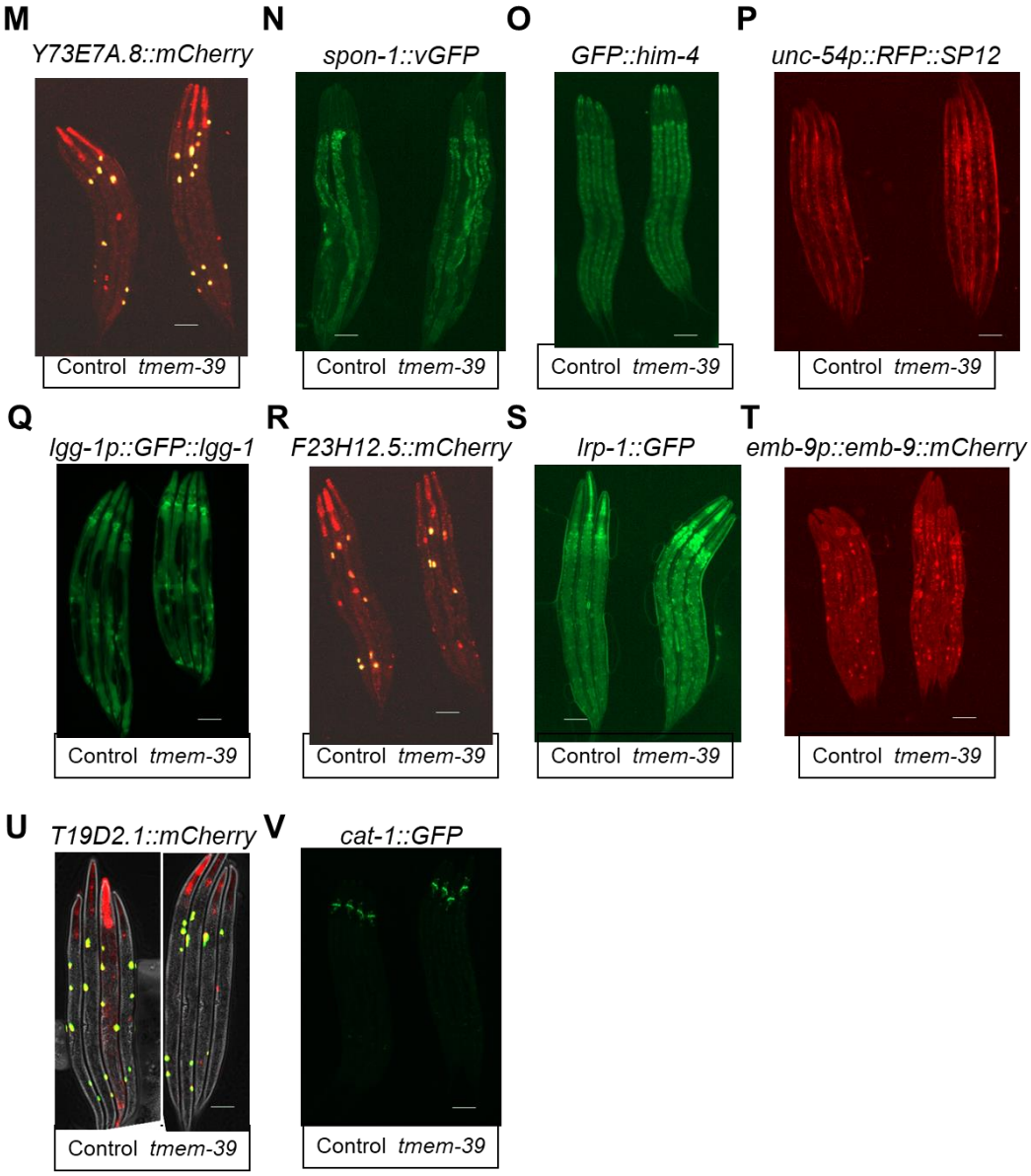

635 **Fig. S1. *tmem-39* RNAi knock-down for screen of phenotypic defects of different**

636 **translational fluorescent reporters.** (A-V), Exemplar fluorescence images showing

637 translational reporters for (A) *wrk-1*, (B*) gna-1*, (C) *hmr-1*, (D) *mans*, (E) *eff-1*, (F-G)

638 *cpl-1*, (H) *mig-23*, (I) *fat-7*, (J) *ced-1*, (K) *egl-20*, (L) *ubiquitin-V*, (M) *Y73E7A.8*, (N)

639 *spon-1*, (O) *him-4*, (P) *SP12*, (Q) *lgg-1*, (R) *F23H12.5*, (S) *lrp-1*, (T) *emb-9*, (U) *T19D2.1*

640 and (V) *cat-1* in wild-type animals by control and *tmem-39* RNAi at 20 °C (n = 3-4 for

641 each reporters). Scale bars: 20 μm.

642

643 **Fig. S2**

644

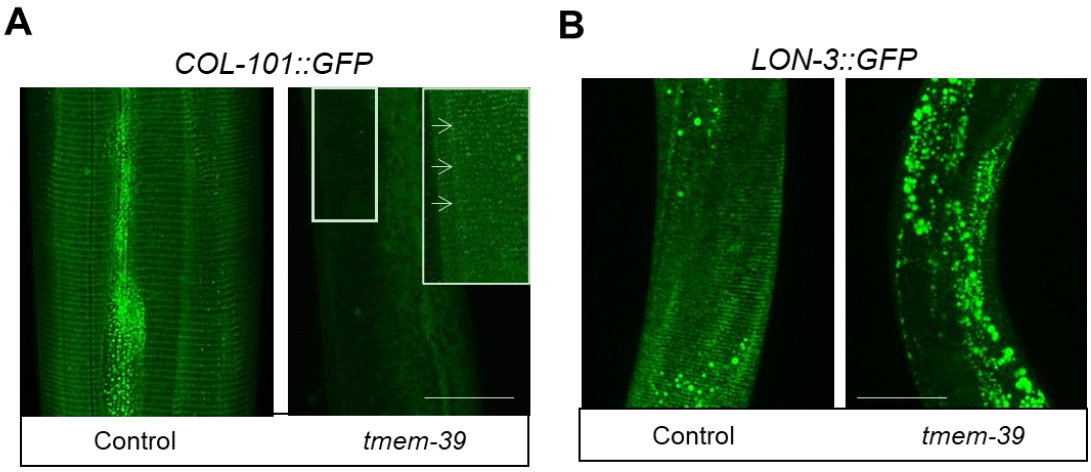

645

646

647

648

649

650 **Fig. S2. *tmem-39* RNAi knock-down other cuticle collagen translational**

651 **fluorescent reporters.** (A-B), Exemplar fluorescence images showing translational

652 reporters for (A) *col-101 and* (B*) lon-3.* In wild-type animals at 20 °C (n = 3-4 for each

653 reporters). Scale bars: 20 µm.

654

655

656 **Fig. S3**

657

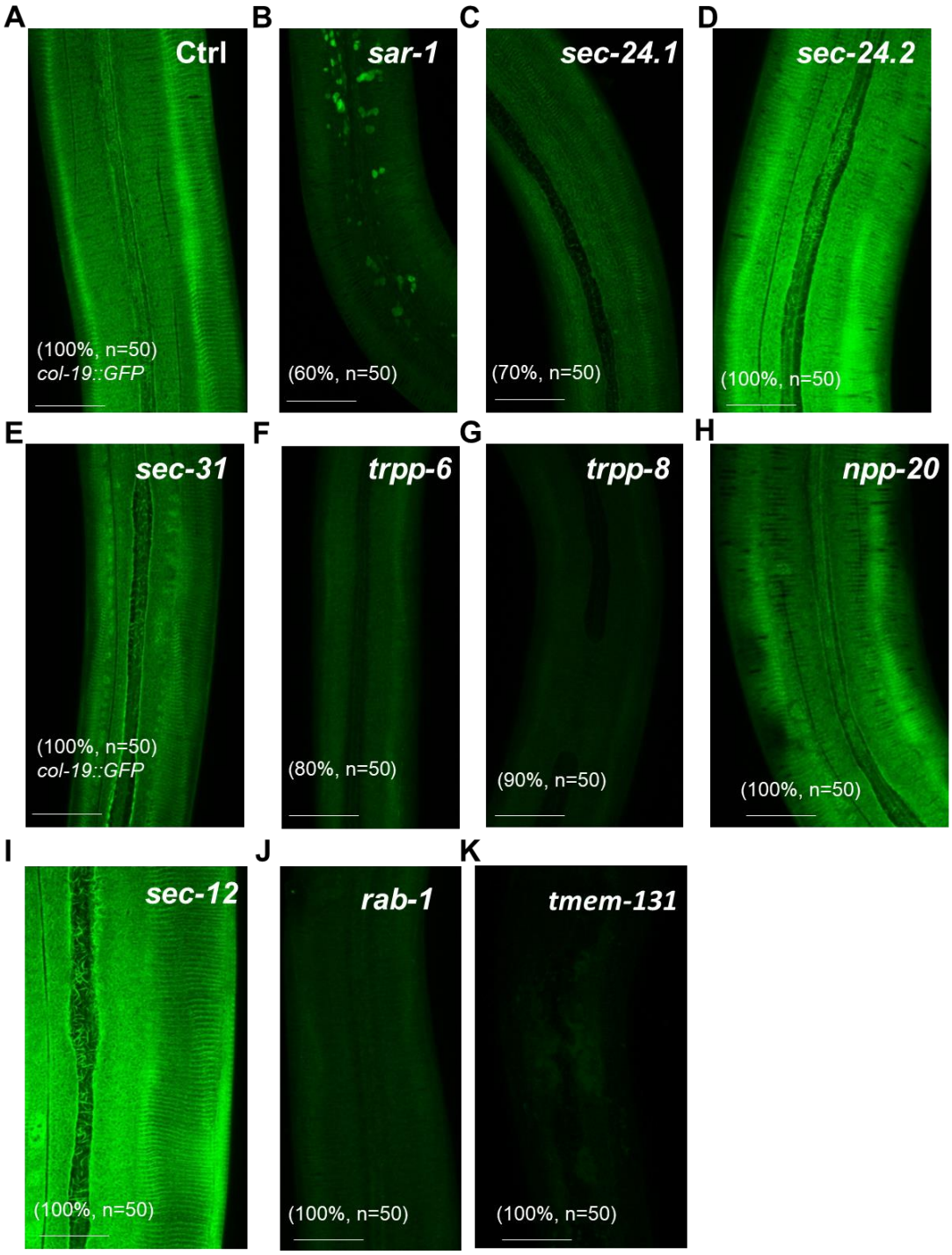

658 **Fig. S3. RNAi knock-down other COP II component genes for screen genes**
659 **involved in collagen production and degradation.** (A-J), Exemplar fluorescence
660 images of *col-19* translational reporter for (A) control, (B) *sar-1*, (C) *sec-24.1*, (D) *sec-*
661 *24.2*, (E) *sec-31*, (F) *trpp-6*, (G) *trpp-8*, (H) *npp-20*, (I) *sec-12,* (J) *rab-1* and (K) *tmem-*
662 *131* RNAi in wild-type animals at 20 °C. Scale bars: 20 μm.

663

664

665 **Fig. S4**

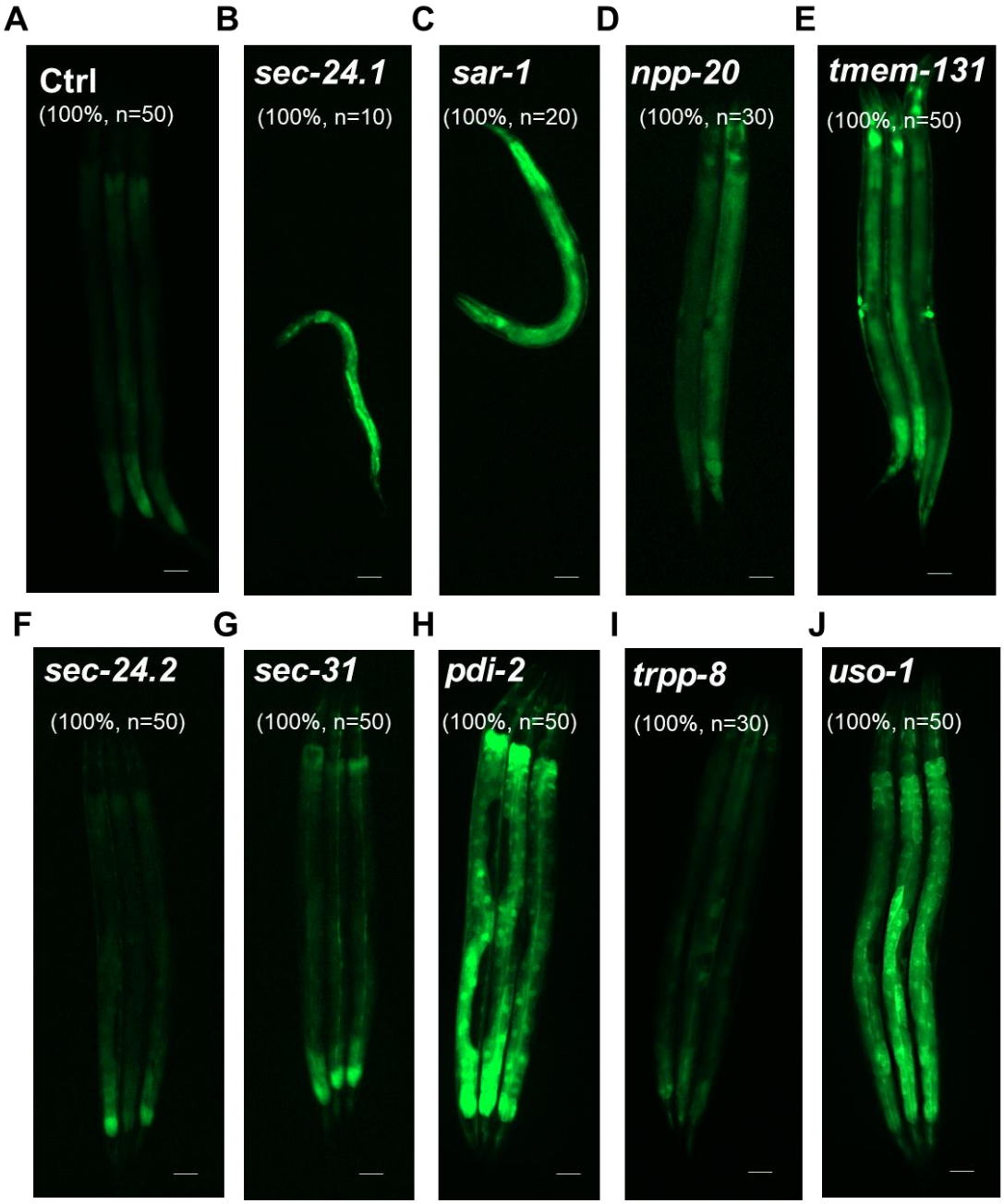

666

667 **Fig. S4. RNAi knock-down COPII component genes for screen genes involved in**

668 **ER stress response.** (A-J), Exemplar fluorescence images of *hsp-4*p::GFP

669 transcriptional reporter for (A) control, (B) *sec-24.1*, (C) *sar-1*, (D) *npp-20*, (E) *tmem-*

670 *131*, (F) *sec-24.2*, (G) *sec-31*, (H) *pdi-2*, (I) *trpp-8* and (J) *uso-1*RNAi in wild-type

671 animals at 20 °C. Scale bars: 20 μm.

672

673 **Table S1A. Primers and oligos used in genomic editing.**

	Primer	Sequence (5'-3')
sgRNA cloning	sgRNA-EcoRI-F	ttgtaaaacgacggccagtgaattcCTCCAAGAACTCGTACAAAAATG
	sgRNA-HindIII-R	ctatgaccatgattacgccaagcttCACAGCCGACTATGTTTG
	TMEM-39 sgRNA1 F:	**GCCGCCTCGAAGACGAGTGC**GTTTAAGAGCTATGCTGGAAACAGC
	TMEM-39 sgRNA1 R:	**GCACTCGTCTTCGAGGCGGC**AAACATTTAGATTTGCAATTCAATTA
	TMEM-39 sgRNA2 F:	**GATCTACGAACCTTCTCAAG**GTTTAAGAGCTATGCTGGAAACAGC
	TMEM-39 sgRNA2 R:	**CTTGAGAAGGTTCGTAGATC**AAACATTTAGATTTGCAATTCAATTA
	TMEM-39 YR sgRNA F:	CCTCCTATTGCGAGATGTCTTG**GCTCGATAGCACCTGCCGTC**GTTTAAGAGCTATGCTGG
Donor oligos	TMEM-39 deletion oligo:	aagatATGCCGCCTCGAAGACGAG^AAGAGGATCTTCTCCTTATGCATCAACTTCAACAAGAACGATAA
	TMEM-39 YR oligo:	ACGCCATGGAGCGAGTTTTGTCTCTATAATGACGGAGAGACTGTTCAAATGCCGGACGGCAGGTGC**GCAGCA**GCCAAATCTTCGAATTCGATAAGAACTGTGGCCGCACATCCGGAAAGTTCTCGGCATAACACTTTCTTTgta

674 Primers were used for PCR with the Addgene plasmid #46169 as template, except YR
675 with the Addgene Plasmid #61253 as template. Bold and underlined are sgRNA target
676 sequence from the *tmem-39* regions. The location of the deleted *tmem-39* is marked
677 with "^", generating a precise 2750 bp deletion. And the nucleotides change for YR
678 codons are labeled in red (**TATCG**A→**GCAGCA**).
679

680 **Table S1B. Primers in Genotyping and RT-PCR.**

	Primer	Sequence (5'-3')
Geno-typing	TMEM-39 Del screen F:	tacagaaccgagaaggtcac
	TMEM-39 Del screen R:	tcacaattgggtagtaccac
	TMEM-39 Del screen R2:	GTGTGAACTGAATATCCGGC
	TMEM-39 YR screen F1:	ATCTTCTACACCGAGCAGCT
	TMEM-39 YR screen R1:	ATGCCGAGAACTTTCCGGAT
	COL-19::GFP screen F：	TTCCAGGACAAAAGGGAGAG
	COL-19::GFP screen R：	TCTCGAGAAGCATTGAACAC
RT-PCR	act-1 RT-F:	CATCCCAGTTGGTGACGATA
	act-1 RT-R:	TCGGTATGGGACAGAAGGAC
	gfp RT-F:	TGTTCCATGGCCAACACTTG
	gfp RT-R:	ACGTGTCTTGTAGTTCCCGT
	gfp RT-R:	ACGTGTCTTGTAGTTCCCGT
	col-19 RT-F:	TACTTGTGTGCGTTCTTGCC
	col-19 RT-R:	TTGGGTTGATGTGCTTGCTC
	tmem-39 RT-F:	GCTTCAATCCCAAGAGCGAG
	tmem-39 RT-R:	GACTTCGGAAGCCACCAAAG

681

682 **Table S2. Reporters examined in phenotypic screen for *tmem-39* RNAi**

Genotype	Reporter	Control	*tmem-39*
hsp-4p::GFP	*hsp-4* transcriptional	*	****
col-19p::col-19::GFP	*col-19* translational	****	*
cat-1p::cat-1::GFP	*cat-1* translational	**	**
eff-1p::eff-1::GFP	*eff-1* translational	*	**
emb-9p::emb-9::mCherry	*emb-9* translational	***	***
lrp-1p::lrp-1::GFP	*lrp-1* translational	**	**
fat-7p::fat-7::GFP	*fat-7* translational	***	***
gna-1p::GFP::gna-1	*gna-1* translational	**	**
him-4p::GFP::him-4	*him-4* translational	**	***
hmr-1p::hmr-1::GFP	*hmr-1* translational	***	***
lgg-1p::mCherry::GFP::lgg-1	*lgg-1* translational	**	**
lim-7p::ced-1::GFP	*ced-1* translational	**	**
myo-3p:: EGFP::wrk-1	*wrk-1* translational	***	****
nhx-2p::cpl-1::YFP	*cpl-1* translational	**	***
nhx-2p::cpl-1(W32A Y35A)::YFP	*cpl-1(W32A Y35A)* translational	***	***
nhx-2p::ubiquitin-V::mCherry	ubiquitin-V proteins	***	***
rpl-28p::F23H12.5::mCherry	F23H12.5 translational	****	****
rpl-28p::T19D2.1::mCherry	T19D2.1 translational	****	****
rpl-28p::Y73E7A.8::mCherry	Y73E7A.8 translational	****	****
spon-1p::spon-1::vGFP	*spon-1* translational	**	**
unc-22p::egl-20::GFP	*egl-20* translational	*	***
unc-54p::RFP::SP12	ER membrane RFP marker	**	***
unc-54p::mig-23::GFP	*mig-23* translational	***	***
vha-6p::mans::GFP	intestinal GFP marker for the Golgi	***	***

683 * indicates fluorescent reporter levels under control and *tmem-39* RNAi conditions;
684 qualitative changes were followed up by quantitative fluorescence (n≥ 20 biological
685 replicates) and Western blot for verification.